Economic Geology
Vol. 96, 2001, pp. 351–366

Chronology of Exotic Mineralization at El Salvador, Chile, by $^{40}Ar/^{39}Ar$ Dating of Copper Wad and Supergene Alunite

TIMOTHY I. MOTE,†

Department of Earth and Planetary Science, University of California at Berkeley, Berkeley, California 94720-4767

TIM A. BECKER, PAUL RENNE,

Berkeley Geochronology Center, 2455 Ridge Road, Berkeley, California 94709

AND GEORGE H BRIMHALL

Department of Earth and Planetary Science, University of California at Berkeley, Berkeley, California 94720-4767

Abstract

Exotic copper mineralization is a complex hydrochemical process linking supergene enrichment, lateral copper transport, and precipitation of copper oxide minerals in the drainage network of a porphyry copper deposit. At the El Salvador porphyry copper deposit in northern Chile the majority of the exotic ore comprised a mixture of copper-bearing manganese oxyhydrates termed "copper wad." X-ray diffraction, scanning electron microscopy, and electron probe microanalysis show that the copper wad is composed of copper-bearing cryptomelane [$K_{1\text{-}2}(Mn^{3+}Mn^{4+})_8O_{16} \bullet xH_2O$] and birnessite [$K_{0.33}Mn^{3.9+}_{7}O_{14} \bullet 7H_2O$] structures. These natural occurrences within the exotic ore provide the opportunity to directly date the formation of these deposits using recent advances in $^{40}Ar/^{39}Ar$ geochronology of supergene K-Mn oxides formed by weathering.

A suite of copper-bearing cryptomelane and birnessite samples from exotic deposits within the El Salvador district were characterized and dated by $^{40}Ar/^{39}Ar$ laser step heating. Supergene alunite [$KAl_3(SO_4)_2(OH)_6$] found in paleospring feeder systems leading from the source zones of copper outward to the exotic mineralization was dated to independently constrain the age of exotic ore formation.

Although the Ar retentivity of the layered birnessite structure has been questioned by others, the Ar retentivity of these samples is thought to be a function of their natural preservation and limited postcrystallization ground-water interaction in the hyperarid Atacama desert. The $^{40}Ar/^{39}Ar$ analytical results show that Ar and/or K losses after crystallization, excess ^{40}Ar, and ^{39}Ar recoil do not pose significant problems; therefore, in the context of exotic copper deposits within hyperarid environments this dating method is applicable to both cryptomelane and birnessite within copper wad.

The $^{40}Ar/^{39}Ar$ dating of exotic mineralization at El Salvador indicates that supergene and exotic mineralization processes were active at ~35 Ma, about 5 m.y. after the emplacement of hydrothermal mineralization, and continued until the middle Miocene. The majority of exotic mineralization extends from the Oligocene-Miocene (24 Ma) boundary through the middle Miocene (11 Ma) and relates to supergene fluid emanating in multiple directions from the source of copper in Indio Muerto, which represents a topographic high above the exotic deposits.

One reconnaissance date of exotic mineralization at the Chuquicamata porphyry copper deposit yielded an age of 17.03 ± 0.03 Ma coincident with the known supergene alunite dates for this deposit. Reconnaissance dating at Exotica-Mina Sur and El Abra proved problematic due to the presence of contaminant silicate minerals within the copper wad.

Ages derived here for exotic mineralization are similar to the known supergene ages throughout northern Chile. The dates indicate that supergene exotic mineralization began at the Eocene-Oligocene boundary and continued through the Oligocene, eventually ceasing in the middle Miocene due to desiccation of the Atacama desert.

A series of 10-cm-thick supergene alunite veins were microsampled across their widths and dated to address the kinetics of alunite vein growth. Apparent growth rates of the veins vary from 71 to 100 mm/m.y. in the horizontal direction to 24 mm/m.y. in the vertical, presumably caused by differences in pressure regimes due to their orientation.

Introduction

EXOTIC copper mineralization is a complex hydrochemical process linking supergene enrichment, lateral copper transport, and precipitation of copper oxide minerals into the drainage network of a porphyry copper deposit. Recent exploration trends target exotic deposits because they are amenable to heap leaching; their sulfide-free copper oxide ore is environmentally benign; and their common occurrence near existing mine infrastructure extends mine life. Although Mote et al. (2001) quantified the fundamental transport and chemical mechanisms controlling the formation of exotic copper deposits, a gap in the genetic model exists as direct knowledge of the timing of these deposits within the geologic record is lacking.

Previous efforts to place exotic deposits in a geochronological context at El Salvador and elsewhere have been indirect

† Corresponding author: e-mail, tim@timote.com

(Münchmeyer, 1996). Since the exotic ore commonly occurs within the Atacama gravels (Sillitoe et al., 1968; Mortimer, 1973), local pyroclastic flows and tuffs within the gravels have been dated at 12.5 ± 0.5 and 11.6 ± 0.5 Ma (Sillitoe et al., 1968) to constrain their formation.

During the formation of exotic mineralization the oxidation of primary sulfides is necessary to generate acid and release copper ions into solution so as to allow fluids to transport copper out into the surrounding paleodrainage network. Therefore, another chronological and geochemical constraint on the age of these deposits is the timing of supergene enrichment in the source region of the exotic deposit. Supergene enrichment in northern Chile has been shown to be related to distinct episodes of descending ground-water table related to Cenozoic tectonic uplift coupled with climatic events (Brimhall and Mote, 1997; Mote and Brimhall, 1997). Alpers and Brimhall (1988) dated the supergene processes at Escondida and concluded that middle Miocene desiccation of the Atacama enhanced supergene processes and then preserved the supergene enrichment blankets as erosion rates plummeted at approximately 14 Ma. Sillitoe and McKee (1996) summarized that supergene enrichment of the Chilean porphyry copper province occurred from 34 to 14 Ma by obtaining K-Ar ages of supergene alunite from deposits and prospects between latitudes 20° and 27° S.

The well-studied El Salvador porphyry copper deposit (Gustafson and Hunt, 1975; Corneja et al., 1997) and exotic mineralization (Carrasco and Rojas, 1993; Rojas and Müller, 1994; Münchmeyer, 1996, Mote et al., 2000) provide a framework to incorporate dating results that constrain exotic ore-forming processes.

Characterization of the exotic ore by X-ray diffraction, scanning electron microscopy, and electron probe microanalysis shows that Cu-rich K-bearing Mn oxyhydrates with cryptomelane and birnessite structures comprise a significant portion of the material termed "copper wad." The natural occurrence of these K-bearing Mn oxyhydrates within the exotic deposits provides the unique opportunity to directly date their formation using recent advances in $^{40}Ar/^{39}Ar$ laser step-heating geochronology of weathering minerals (Vasconcelos et al., 1994). This is a novel application of $^{40}Ar/^{39}Ar$ dating on K-bearing Mn oxyhydrates that form copper wad and provided the first dates obtained from an actual copper-bearing ore mineral within an exotic copper deposit.

The age of supergene alunite found in the paleospring feeder systems leading from the source regions of copper out to the exotic ore (Mote et al., 2001) provides an independent check on the copper wad geochronology.

Geologic Setting

The El Salvador porphyry copper deposit is located in the Indio Muerto district of the Atacama desert of northern Chile (26° 15' S lat), 800 km north of Santiago (Fig. 1). The deposit is located near the southern segment of the Domeyko fault system, a trench-linked strike-slip fault system whose activity was contemporaneous with emplacement of numerous middle Eocene to early Oligocene porphyry Cu-Mo deposits in the Andean pre-Cordillera of northern Chile (Cornejo et al., 1997).

The mineralized porphyries intruded into a Paleocene rhyolitic dome complex, Cerro Indio Muerto, during a 3 m.y. period from 44 to 41 Ma (Cornejo et al., 1997). The main Cu-Mo porphyry intruded the Quebrada Turquesa area of Cerro Indio Muerto during a ~1 m.y. period (42–41 Ma). The magmatic history of the system culminated with the intrusion of latite dikes into a postore district-scale northwest-trending fault system (refer to Gustafson and Hunt, 1975; Gustafson and Quiroga, 1995; Cornejo et al., 1997; Gustafson et al., 2001; for further details on the geology, hypogene mineralization processes, and geochronology).

Soon after the hypogene mineralization at El Salvador, supergene enrichment commenced due to a decent in the ground-water table, spurred by tectonic uplift and episodic

FIG. 1. Plan map of northern Chile, showing the major porphyry copper districts. Deposits examined in this study are El Salvador, Chuquicamata, and El Abra.

climate changes (Brimhall and Mote, 1997; Mote and Brimhall, 1997). These climatic changes continued well into the middle Miocene and created an environment conducive to sulfide oxidation above the ground-water table (Alpers and Brimhall, 1988). The supergene enrichment processes created an economic enrichment blanket of 300 million tons (Mt) of copper ore with an average grade of 1.6 wt percent in 1959 when the mine was put in production (Gustafson and Hunt, 1975). Two prior studies constrained the supergene enrichment at El Salvador: Gustafson and Hunt (1975) obtained two dates of 36.1 ± 0.6 and 36.0 ± 2.5 Ma on supergene alunite, and Sillitoe and McKee (1996) published one date of 23.1 ± 0.7 Ma for supergene alunite from the leached capping. Both studies used K-Ar dating methods.

Regional lateral flow of copper-bearing fluids

During the supergene enrichment process Cu-bearing fluids acquired a lateral-flow component and escaped the principal deposit from two distinct district-scale latite dike sets, which intruded presupergene age faults. These latite dike structures had higher permeability than adjacent wall rock and concentrated the flow of acidic copper-bearing fluids through an unreactive protore assemblage, which allowed the fluids to emanate from a paleospring feeder system located at a 2,690-m elevation in Quebrada Riolita, overlooking the Damiana deposit (Mote et al., 2001). The paleospring feeder environments are characterized by abundant gravels cemented by a jarosite [$KFe_3(SO_4)_2(OH)_6$] matrix and 10-cm-thick veins filled with supergene alunite. The term "supergene alunite" is used in this sense to imply that the alunite veins are formed from supergene fluids transported a distance from the original source of oxidizing sulfide and is analogous to "transported" or "exotic" limonite from Anderson (1982). The low pH, copper-rich fluids followed hydraulic gradients moving away from the principal deposit, flowing in gravel-covered paleochannels until an effective geochemical barrier caused hydrolysis reactions to occur between the acidic fluids and the andesite basement of the channel. These reactions neutralized the acidic fluid, increased the pH, and caused copper ore minerals to reach saturation and precipitate in fractures of the basement rock, thereby creating an exotic copper orebody (Mote et al., 2001). The exotic ore consists mostly of copper wad with lesser amounts of chrysocolla, turquoise, and malachite.

Starting from the source of copper within the topographically high Indio Muerto, the exotic mineralization extends underneath alluvial fans in multiple directions as far as 8 km away (Fig. 2). The presently known exotic deposits at El Salvador (Damiana (Münchmeyer, 1996; Fam et al., 1997), Quebrada Turquesa (Mote et al., 2001), and Exotica Alicia (Pino, 1997)) all lie within drainages that source at the intersection of the topography and northwest-striking district-scale latite dikes. These intersections formed paleospring feeder systems on the flanks of Cerro Indio Muerto where Cu-bearing acidic fluids emerged from the subsurface (Mote et al., 2001).

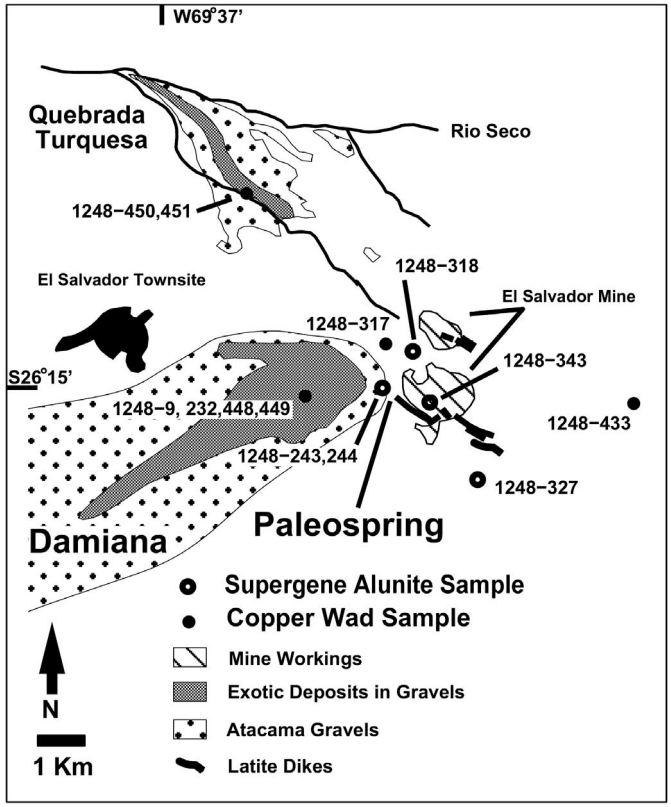

FIG. 2. Plan map of the El Salvador district, showing the known exotic deposits. Circle symbols delineate the samples used in this study.

Copper Wad Characterization

Manganese oxyhydrates are common weathering products and occur in a wide variety of geologic environments (Post and Veblen, 1990). The incorporation of metals such as Cu, Zn, and Co into the Mn oxyhydrate structure can commonly form economic minerals. Copper wad is the mining term for a mixture of these copper-bearing Mn oxyhydrates whose crystal structure proves difficult to accurately characterize. It is this incorporation of variably sized metal cations into the Mn oxyhydrate structure that changes the d-spacing of the crystal lattice and produces diffuse X-ray diffraction patterns; the term copper wad is thus somewhat generic. Copper wad occurs naturally as a dull black friable material filling void space in fractured altered host rock or as a matrix cementing gravels in a paleochannel. Its occurrence has been reported in numerous world-class copper districts such as Butte, Montana (Smith, 1941) and Chuquicamata's Exotica deposit (Mortimer et al., 1977; Fam, 1979).

Collection

Difficulties in dating weathering products, such as K-bearing Mn oxyhydrates, arise from contamination of the sample of interest by the older host or parent material, causing mixed ages; therefore, a requirement for dating these minerals is the collection of homogenous samples free of contaminant minerals. Void spaces or open fractures within the host rock provide an ideal place for these homogeneous minerals to grow freely and thickly. Natural exposures of copper wad filling fractures or veins are rare as they are commonly covered with colluvium. Man-made exposures such as open pits, road cuts, trenches, and shafts, however, provide an excellent opportunity to find appropriate material.

At El Salvador, the most promising copper wad samples were collected from underground workings within the central portion of the orebodies where they filled void spaces in veins. In general, the collected samples included the vein and host rock, allowing for detailed separation in the laboratory. Sample locations for copper wad collected are noted in Figure 2.

Preparation

Sample preparation is an essential step in dating these minerals, as one needs to visually separate enough homogeneous material for optical microscopy, X-ray diffraction, electron probe microanalysis, scanning electron microscopy, and $^{40}Ar/^{39}Ar$ dating. Copper wad samples were prepared three ways: an in situ whole-rock sampling method, a mineral isolation technique, and a hydrofluoric acid (HF) leaching method.

In situ sample preparation involved mounting the sample (including host rock and copper wad vein) onto a glass slide and then cutting it to a 1-mm thickness and polishing it for reflected light microscopy. This method is useful to identify growth bands and analyze any contamination between the host material and the copper wad. Removal of the sample involved separating specific phases of the sample with a microsaw, followed by dissolution of the Crystal Bond™ adhesive with acetone. The main advantage of this method is the ability to separate individual bands thick enough to be dated. The drawback lies in that it is a delicate and time-consuming method.

The mineral separation method used a tungsten carbide tip pointer to free the thickest copper wad material from the host rock. This material was then placed in a mortar and pestle where a light pressure was applied, which slightly crushed the material. This separated the hardest, most crystalline phases from the soft altered andesite host rock that may contaminate the copper wad analysis. The most crystalline wad is favorable for radiogenic dating, as the integrity of its crystal structure is essential for Ar retention. The grains were washed in distilled water and examined under a microscope. Using steel tweezers, the visually most uncontaminated grains were handpicked and then cleaned in an ultrasonic bath for approximately 1 min to remove any loose material. Sample sizes are roughly 1-mm-diameter spheres. Sample grains were mounted in epoxy and polished for optical microscopy and electron probe microanalysis. Mineral separation was the most commonly used method, as it yielded an ample amount of pure material. The drawback of this method was that separation of individual bands was not feasible using this approach.

The third technique used hydrofluoric acid (HF) to attempt to separate the copper wad from the silicates in the host rock. The $^{40}Ar/^{39}Ar$ analyses showed that no Ar was retained in the leach residue; therefore, we infer that this leaching method destroyed the Mn oxyhydrate structure, as previously shown by Vasconcelos et al. (1994).

Characterization

Polished samples of copper wad were examined by reflected light microscopy and show mammilary growth bands (Fig. 3). The optically homogeneous continuous bands clearly formed as episodic open-space filling.

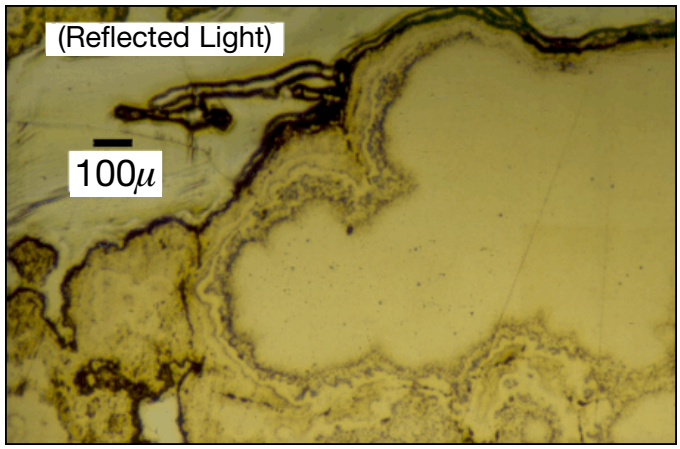

FIG. 3. Photomicrograph of a polished copper wad sample 1248-9 in reflected light, showing mammillary growth bands. Bands widths are approximately 25 μm thick.

The introduction of metals such as Cu, Co, and Zn into manganese oxyhydrates forming copper wad makes the identification of copper wad by X-ray diffraction difficult as variations in d-spacing from compositional changes produces diffuse patterns. Extended scans, on the order of 12 h, were more effective. The X-ray diffraction analysis of several samples showed evidence of two distinct structures in the copper wad: cryptomelane with the hollandite structure (Vasconcelos et al., 1994) and birnessite with the phyllomanganate structure (Holland and Walker, 1996). The discrimination between the two structures is problematic as it is based on weaker secondary and tertiary diffraction peaks as both minerals have a primary peak at 12.5° (2ν).

The scanning electron microscopy (SEM) analysis of copper wad showed that birnessite is the major component of the copper wad sampled at El Salvador, as it was found in all the samples except 1248-433. Birnessite in a layered structure was occasionally found with a turbostratic stacking structure (Holland and Walker, 1996) where rotated layers are stacked on top of each other. Cryptomelane in the hollandite structure (2 × 2 tunnels) was identified as a minor component of the copper wad in sample 1248-232, approximated to represent 10 vol percent, and in samples 1248-448 and 1248-449 as rare micron-scale crystals. Sample 1248-433 was found to be composed of chalcophanite and cryptomelane in approximately equal proportions. Refer to Mote (1999) for further details, including photomicrographs, on the scanning electron microscopy analysis of copper wad mineralogy.

Scanning electron microscopy coupled with electron dispersive microprobe analysis was used to identify the existence of microscopic contaminant grains within the samples. Numerous submillimeter-scale grains of K silicate minerals were found imbedded within sample 1248-336. The analysis showed that hydrothermal sericite is intermixed with copper wad in sample 1248-QD-168.

Electron probe microanalysis was performed to determine elemental concentrations of K within the copper wad from homogeneous bands (i.e., Fig. 3) identified by optical microscopy (Table 1). The majority of the copper wad contains greater than 1 wt percent K, reaches a maximum of over 3 wt

TABLE 1. Summary of Electron Probe Microanalyses (wt %)

Sample no.	K	Cu	Co	Mn	O	Si	Fe	Zn	Al	Ca	Na	Ba	Mo	S	Totals
1248-9	0.90	16.72	1.04	41.21	32.43	0.38	0.91	NA	0.25	0.16	0.17	0.67	NA	0.07	95.26
1248-9	1.52	10.71	1.00	42.75	31.64	0.92	0.48	NA	0.89	0.32	0.29	1.12	NA	0.05	92.04
1248-9	2.73	6.35	2.85	46.89	34.64	1.03	0.01	NA	0.24	0.25	0.22	0.19	NA	0.00	95.55
1248-448	1.90	7.59	0.70	44.72	33.40	1.07	1.12	0.27	1.56	0.53	0.40	0.27	NA	0.08	94.02
1248-449	2.63	4.58	0.38	48.49	35.26	0.31	0.11	0.45	1.25	0.44	0.35	0.16	NA	0.04	95.36
1248-449	2.89	3.39	0.25	50.57	34.42	0.22	0.41	0.61	0.95	0.39	0.30	0.22	NA	0.03	95.43
1248-232	0.19	21.86	0.07	34.10	33.34	1.66	0.17	0.33	0.27	0.32	0.24	0.39	0.18	0.24	93.47
1248-232	0.81	17.91	0.65	37.88	28.35	0.39	0.06	0.20	0.10	0.07	0.11	0.01	0.06	0.00	86.68
1248-232	0.93	14.17	0.86	39.88	34.17	0.33	1.08	0.89	0.17	0.22	0.16	0.36	0.00	0.00	93.48
1248-232	2.52	4.24	0.20	49.05	34.97	0.19	0.19	3.01	0.76	0.14	0.05	0.65	0.01	0.00	96.10
1248-232	3.29	2.53	0.11	50.26	33.87	0.32	0.06	3.40	0.99	0.13	0.05	0.97	0.03	0.00	96.17
1248-450	1.33	7.65	2.32	42.52	30.51	0.41	1.54	0.35	0.11	0.54	1.09	0.18	0.00	0.05	89.07
1248-451	1.52	5.74	1.40	41.81	30.77	0.72	2.56	0.40	0.73	0.31	0.86	0.63	0.00	0.25	88.50
1248-317	2.86	1.92	0.18	47.19	33.99	0.47	4.02	0.27	0.99	0.83	0.29	0.88	0.07	0.00	94.13
1248-433	0.05	0.01	0.02	46.07	30.64	0.13	0.01	17.14	0.07	0.04	0.00	0.03	0.02	0.00	94.30
1248-433	1.08	0.07	0.01	49.09	32.36	0.22	0.02	12.97	0.04	0.05	0.00	0.00	0.00	0.00	95.91
1248-433	1.34	0.05	0.08	48.58	35.05	0.17	0.17	7.16	0.07	0.36	0.19	0.12	0.02	0.08	93.57
1248-QD-168	2.42	7.10	1.00	46.12	33.83	0.30	1.17	0.09	0.67	0.27	0.20	0.65	0.20	0.01	94.14
1248-QD-168	2.80	4.94	0.74	49.45	34.72	0.18	0.39	0.10	0.99	0.39	0.16	1.24	0.08	0.01	96.33
1248-QD-89	3.48	2.59	0.14	52.57	34.89	0.67	0.70	0.35	1.20	0.10	0.46	0.04	0.03	0.06	97.34

Notes: Analyses were performed on a Cameca SX-51, 15 KeV with 15 second count times
Refer to http://perry.geo.berkeley.edu/geology/labs/epma/index.htm

percent, and therefore is potentially amenable to $^{40}Ar/^{39}Ar$ dating. Cu concentrations in these samples reach over 20 wt percent. Co reaches a maximum of 3 wt percent in certain samples, although always isolated in individual growth bands. Zn is found up to 17 wt percent in one sample with almost no Cu. The low totals ranging from 86 to 97 wt percent are due to water trapped between layers, which is volatized under the electron beam. Some phases of birnessite have up to 7 stoichiometric molecules of H_2O within their structure and permit a possible loss of up to 14 wt percent (Post and Veblen, 1990).

Factor analysis of the probe data identifies substitution trends useful in describing the incorporation of Cu in the Mn oxyhydrate structure creating copper wad. Probe data were separated into two groups based on mineralogic identification. The probe data confirmed that cryptomelane has 2.2 to 3.5 wt percent of K and varying amounts of Mn, Cu, and Co, whereas the K content in birnessite varies. The factor analysis showed that Mn anticorrelates with the Cu and Co, which implies the basis of substitution in the structure. In the birnessite structure Cu anticorrelates with both K and Mn, whereas Co anticorrelates with Mn. This implies that in the layered birnessite structure Co substitutes for Mn and Cu can substitute for both Mn and K. In the hollandite structure Cu can substitute for Mn (in the octahedral site) or K (in the A cations site; Vasconcelos et al., 1994).

Ideally one would want to separate the most K rich phases as identified by the probe data for $^{40}Ar/^{39}Ar$ analysis. Unfortunately, due to the ~20-μm width of individual growth bands separation of individual phases is unfeasible. Discussion of the implications of the dating results due to compositional variations is deferred to a later section.

Supergene Alunite Characterization

Collection

Samples of supergene alunite were chosen to represent paleospring feeder systems connecting copper source zones with the multiple exotic deposits (Fig. 2). The open-space fracture filling by supergene alunite in these zones allowed for relatively clean sample separation.

Preparation

The durable porcelaneous texture of the alunite samples allowed detailed microsawing of numerous 1-mm-cubed samples traversing a 10-cm-wide vein. Two sample traverses were made with four samples in each traverse (1248-243A, B, C, D and 1248-244A, B, C, D). Individual samples are spaced about 2 cm apart.

Characterization

Optical microscopy of the supergene alunite under transmitted light shows a microcrystalline sugary texture distinctive of supergene or low-temperature secondary phases, with crystals <10 μm in length (Itaya et al., 1996). Scanning electron microscopy of sample 1248-244 confirms the <10-μm dimension of a euhedral alunite crystal (Mote, 1999).

X-ray diffraction analysis on the samples shows that the major mineral phase is alunite with minor intermixtures of montmorillonite clay and jarosite, which are not apparent in the thin section. Previous workers showed that clay can cause significant Ar recoil effects (Huneke and Smith, 1976), but leaching the alunite in hydrofluoric acid (HF) can remove all of the clays and retain the trapped Ar (Itaya et al., 1996). Hydrofluoric acid leaching of supergene alunite was not preformed in this study as the clay intermixing was interpreted as minute.

Electron microprobe analysis of the supergene alunite shows that the alunite is relatively homogeneous and has approximately 6 wt percent K.

$^{40}Ar/^{39}Ar$ Analysis

Grains of both copper wad and supergene alunite samples were placed in aluminum disks along with a sanidine from the

Fish Canyon tuff as neutron fluence monitor (Renne et al., 1998), wrapped in Al foil, and packed in quartz tubes for irradiation. Four separate sample groups were irradiated for 7, 3.5, 10, and 7 h at the Triga Reactor at Oregon State University. Nucleogenic production of ^{36}Ar, ^{39}Ar, and ^{40}Ar from nuclear reactions involving K and Ca was corrected using data of Renne et al. (1998). After a 3- to 6-mo cooling period, the samples were baked out at 200°C for 8 h, pumped down to an ultrahigh vacuum, and then step heated under a continuous Ar ion laser with defocused beam. The fraction of gas released was cleaned through a cyrocooled cold trap (T = –140°C) and SAES ST-101 Zr-Al getters, then analyzed for argon isotopes in an MAP 215C mass spectrometer. Analytical procedures followed are described in Vasconcelos et al. (1994). Data collected for mass discrimination, nucleogenic interference, and atmospheric contamination were used to calculate apparent ages for each degassing step. Age uncertainties are reported as 1σ and do not include uncertainties in data for standards, decay constants, or fluence monitor.

Results

Age spectra derived from laser step heating are presented in Figure 4A-C. A summary of the sample characterization, location, and dating results are listed in Table 2, and the analytical data are shown in Appendix 1. Plateau definitions were defined by using the criteria from Fleck et al. (1977): over 50 percent of the gas in three consecutive continuous steps within 95 percent confidence level. The majority of age spectra presented for the samples enable definition of plateaus and reveal initial $^{40}Ar/^{39}Ar$ values of 295.5, suggesting that inherited argon is not present. The four samples that did not enable the plateau definition (1248-317-A, 1248-450, 1248-433, 1248-QD89) did in fact reach a psuedoplateau with over 50 percent of the gas on only two steps. Sample 1248-343 did not reach a plateau.

El Salvador district

Figure 5 shows the location of $^{40}Ar/^{39}Ar$ ages determined in this study. The samples were chosen from distinct areas

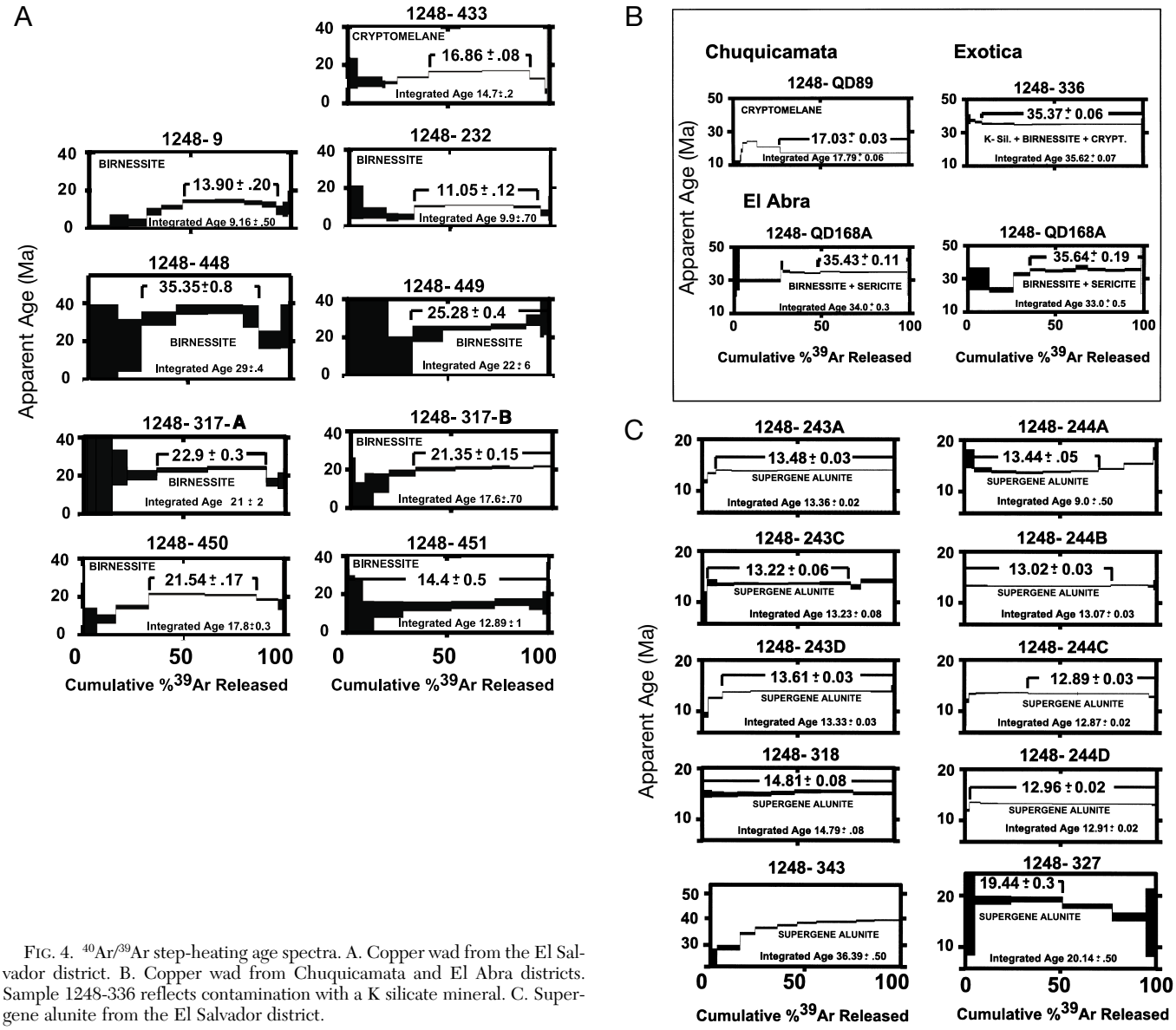

FIG. 4. $^{40}Ar/^{39}Ar$ step-heating age spectra. A. Copper wad from the El Salvador district. B. Copper wad from Chuquicamata and El Abra districts. Sample 1248-336 reflects contamination with a K silicate mineral. C. Supergene alunite from the El Salvador district.

TABLE 2. Summary of Samples

Sample no.	Material	Enrichment environment	Location	UTM coordinates			Summary of dating results: Plateau BGC lab no.	Error age (Ma)	(Ma)
El Salvador district									
1248-9	Birnessite	FA	ES - Damiana	442159E	7096125N	2555m	10237-01	13.90	0.20
1248-232	~90% birnessite, 10% cryptomelane	FA	ES - Damiana	442159E	7096125N	2555m	10287-01	11.05	0.12
1248-317-A	Birnessite	FA	ES - Quebrada Turquesa	443561E	7097029N	2660m	11023-01	22.90	0.30
1248-317-B	Birnessite	FA	ES - Quebrada Turquesa	443561E	7097029N	2660m	11023-02	21.35	0.15
1248-433	Chalcophanite, cryptomelane	FA	ES - Quebrada Cinc	447235E	7096015N	2590m	11121-02	16.86	0.08
1248-448	Birnessite >> cryptomelane	FA	ES - Damiana	442159E	7096125N	2555m	10305-01	35.35	0.80
1248-449	Birnessite >> cryptomelane	FA	ES - Damiana	442159E	7096125N	2555m	10305-02	25.28	0.40
1248-450	Birnessite	FA	ES - Quebrada Turquesa	440827E	7100258N	2330m	11021-02	21.54	0.17
1248-451	Birnessite	FA	ES - Quebrada Turquesa	440827E	7100258N	2330m	11029-02	14.40	0.50
1248-243A	Supergene alunite	FR	ES - Quebrada Riolita	442991E	7096242N	2690m	10316-01	13.48	0.03
1248-243B	Supergene alunite	FR	ES - Quebrada Riolita	442991E	7096242N	2690m	NA	NA	NA
1248-243C	Supergene alunite	FR	ES - Quebrada Riolita	442991E	7096242N	2690m	10315-01	13.22	0.06
1248-243D	Supergene alunite	FR	ES - Quebrada Riolita	442991E	7096242N	2690m	10317-01	13.61	0.03
1248-244A	Supergene alunite	FR	ES - Quebrada Riolita	442991E	7096243N	2690m	10310-02	13.44	0.05
1248-244B	Supergene alunite	FR	ES - Quebrada Riolita	442991E	7096243N	2690m	10311-01	13.02	0.03
1248-244C	Supergene alunite	FR	ES - Quebrada Riolita	442991E	7096243N	2690m	10312-01	12.89	0.03
1248-244D	Supergene alunite	FR	ES - Quebrada Riolita	442991E	7096243N	2690m	10313-01	12.96	0.02
1248-318	Supergene alunite	FR	ES - Quebrada Turquesa	443937E	7096975N	2750m	11044-01	14.81	0.08
1248-327	Supergene alunite	FR	ES - Quebrada Agolomorado	445400E	7094230N	2950m	11053-01	19.44	0.30
1248-343	Supergene alunite	FR	ES - Indio Muerto	444899E	7095863N	3150m	11037-01	NA	NA
Chuquicamata District									
1248-QD-89	Cryptomelane	FP	Chuquicamata[1]	510340E	7537295N	2940m	11026-02	17.03	0.03
1248-336	K-silicate/birnessite/ cryptomelane	GM	Mina Sur / Exotica	NA	NA	NA	11036-04	35.37	0.06
El Abra District									
1248-QD-168B	Birnessite/hydro-thermal sericite	GM	El Abra[1]	515880E	7575420N	3870m	11025-04	35.63	0.19
1248-QD-168A	Birnessite/hydro-thermal sericite	GM	El Abra[1]	515880E	7575420N	3870m	11025-03	35.42	0.11

[1] Collected by John Dilles

Abbreviations: FA = Fractures within andesite, FP = Fractures within poryphyry, FR = Fractures within rhyolite capping, GM = Gravel matrix

thought to be significant to characterization of the escape of copper-bearing fluids and exotic mineralization in multiple directions from the principal deposit.

Copper wad samples within Damiana come from an exploration shaft within the central and most economic portion of exotic mineralization. This shaft exposes a vertical segment of mineralization where copper wad composed of both cryptomelane and birnessite has filled fractures within the altered andesite. The $^{40}Ar/^{39}Ar$ dating results from these samples yield plateau ages of 35.35 ± 0.8 (1248-448), 25.28 ± 0.4 (1248-449), 13.9 ± 0.2 (1248-9), and 11.05 ± 0.12 Ma (1248-232).

Alunite samples from the Damiana paleospring feeder system, at 2,690-m elevation, were sampled from two crosscutting orthogonal faults. The samples come from 10-cm-thick alunite veins exposed by a road cut within 100 m of the outcrop of the latite dike. Microsampling across the alunite veins allowed examination of the growth history of alunite in differently oriented veins. The horizontal vein yielded plateau ages of 13.44 ± 0.05 (1248-244A), 13.02 ± 0.03 (1248-244B), 12.89 ± 0.03 (1248-244C), and 12.96 ± 0.02 Ma (1248-244D) across the width of the vein, whereas the vertical vein yielded plateau ages of 13.43 ± 0.03 (1248-243A), 13.22 ± 0.06 (1248-243C), and 13.61 ± 0.03 Ma (1248-243D).

Copper wad was sampled from Quebrada Turquesa from two distinct areas. A sample from a birnessite-rich copper wad vein exposed at 2,660-m elevation by a road cut in the headwaters of Quebrada Turquesa proximal to the paleospring feeder system, and the original source of copper yielded 2 plateau ages of 22.9 ± 0.30 (1248-317-A) and 21.35 ± 0.15 Ma (1248-317-B). In lower Quebrada Turquesa two birnessite samples yielded plateau ages of 21.54 ± 0.17 (1248-450) and 14.4 ± 0.5 Ma (1248-451) from separate copper wad veins within the mineralized paleochannel exposed by an exploration trench over 3 km from the source of copper. Note that a portion of the mineralized paleochannel has been eroded away, leaving the mineralization in Quebrada Turquesa disconnected from its paleospring feeder system (Mote et al., 2001). Supergene alunite from a vein outcrop at 2,750-m elevation in the headwaters of Quebrada Turquesa

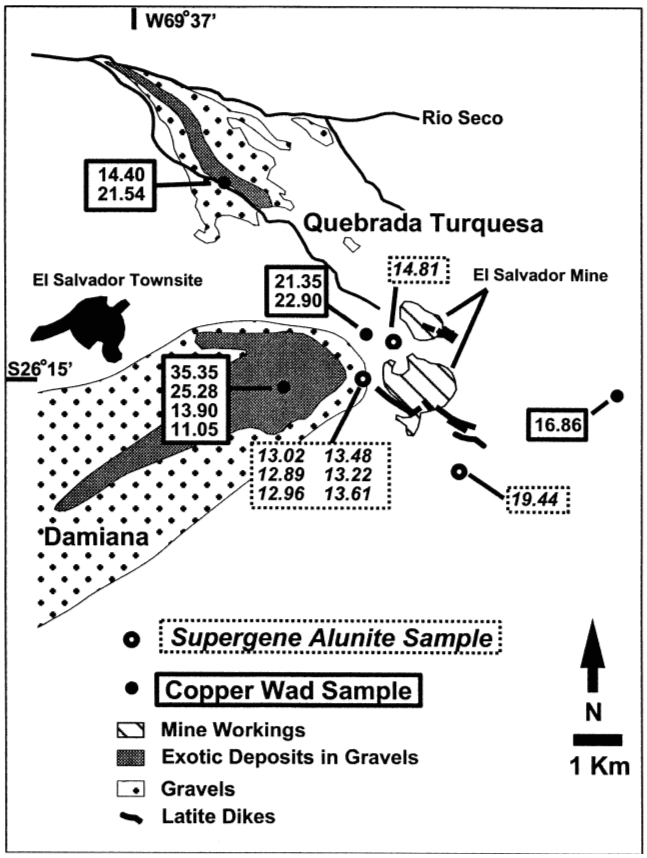

FIG. 5. Plan map of the El Salvador district with calculated plateau ages for samples analyzed. Notice the multiple dates from single-sample locations and the correlation between the dates of the supergene alunite from the paleospring feeder system and the same dates of copper wad from the exotic deposits.

yields an age of 14.81 ± 0.08 Ma (1248-318) and provides independent evidence that acidic fluids escaped from the paleospring feeder system of Quebrada Turquesa at this time.

On the east side of Indio Muerto, Zn-rich Mn oxyhydrate with the phyllomanganate structure, chalcophanite, with intergrown cryptomelane was sampled and dated from a mineralized vein exposed by a younger channel at 2,590-m elevation. This sample shows that supergene mineralization processes were active at 16.86 ± 0.08 Ma (1248-433) in this area.

Supergene alunite from the paleospring feeder system at 2,950-m elevation in the headwaters of Quebrada Algomorado and leading to the Exotica Alicia mineralization to the southeast of Indio Muerto shows enrichment processes active at 19.44 ± 0.3 Ma (1248-327).

Chuquicamata district

Exotica-Mina Sur: The Exotica-Mina Sur copper deposit in the northern Atacama desert of Chile (Fig. 1; Mortimer et al., 1977; Fam, 1979; Münchmeyer, 1996) is the exotic mineralization related to the southern drainage of copper-bearing fluids from the Chuquicamata porphyry copper deposit along the West fissure. Copper wad (1248-336) was sampled on Bench 2415, from an intense alteration zone in the center of a gravel-covered paleochannel on the southeast end of the pit, where copper wad forms a replacement matrix around the gravels. Fresh gravel clasts still exist in this zone, showing that replacement has not been complete.

Figure 4B shows the age spectra of the Exotica deposit, with a plateau yielding an apparent age of 35.37 ± 0.06 Ma (1248-336). This date reflects contamination from older K silicate minerals in rock fragments as it yielded a plateau age coincident with that of the hypogene alteration and mineralization at Chuquicamata from 36 to 31 Ma (Reynolds et al., 1998). Scanning electron microanalysis confirms that micron-scale grains of K silicate mineral are imbedded in the copper wad (Mote, 1999). We interpret that the plateau age for sample 1248-336 is not representative of exotic mineralization.

Chuquicamata: Copper wad was collected by John Dilles from a vein within the altered Este Porphyry exposed by a bench within about 100 m from the top of the Chuquicamata pit. Characterization proved that this sample of copper wad is comprised of mainly the cryptomelane phase. This sample (1248-QD89) is on the north-northwest end of the pit, approximately 20 m east of the Falla Oeste (West fissure), and yields a plateau age of 17.03 ± .03 Ma. The initial hump in the spectrum (Fig. 4B) is thought to be due to an older contaminant phase or recoil effect (Huneke and Smith, 1976). The spectrum flattens out and reaches a plateau for two steps with over 50 percent of the gas and is considered to represent one age of supergene exotic enrichment processes at Chuquicamata.

El Abra district

A copper wad sample (1248-QD168) was collected by John Dilles from the matrix of a 2-m-thick unit of interbedded conglomerate and sandstone, lying on top of the Abra granodiorite. This outcrop is approximately 3 km down the paleohydrologic gradient southwest from the center of the El Abra porphyry copper deposit and 50 m to the east of a fault strand of the Falla Oeste (West fissure). Optical characterization of the sample shows that it is riddled with light-colored contaminant material. Scanning electron microscopy coupled with electron dispersive microprobe analysis show that hydrothermal sericite is intermixed with birnessite layers in the sample (Mote, 1999).

Separation of the copper wad from the hydrothermal sericite was attempted by visually choosing grains free of the contaminant material. Dating of this sample (1248-QD168) yields two plateau ages within analytical error of each other (35.43 ± 0.11 and 35.64 ± 0.19 Ma). This age is in agreement with dates of the hydrothermal sericite alteration event at El Abra (Dilles, pers. commun., 1998) and is not considered to be derived from exotic mineralization. Initial steps in these samples may be representative of degassing from the younger birnessite-comprised copper wad and report apparent ages of 30.18 ± 0.5 (11025-03C, 1248-QD-168A), 30.17 ± 3.5 (11025-04A, 1248-QD-168B), 23.29 ± 0.8 (11025-04B, 1248-QD-168B), and 32.97 ± 0.6 Ma (11025-04C, 1248-QD-168C). These steps, while reporting a geologically reasonable age for exotic mineralization at El Abra, do not reach a plateau and must be considered mixtures of the younger birnessite age and the older hydrothermal sericite age.

Alunite Vein Growth

To address the kinetics of supergene alunite vein growth and the crosscutting relationship between two of these structures, alunite veins from El Salvador were microsampled across their widths and dated. Figure 6 is a photograph of a roadcut exposing these alunite-filled faults in the headwaters of Quebrada Riolita. Figure 7 shows the spatial relationship of the samples and reports the plateau ages summarized in Table 3. For the analysis the assumption was made that the veins represent continuous growth of a homogeneous material. Although sample 1248-244A satisfies the plateau definition it was excluded from this detailed analysis as its plateau age exceeds the integrated age and it shows a saddle-shaped age spectrum dissimilar to the other spectra from this area, although the integrated age of the sample is in close agreement with the other dates. This is due to slight recoil effects from clay contamination, possibly due to the sample proximity to the vein-rock contact, allowing a possible secondary mineralization event to affect it. Montmorillonite is susceptible to recoil effects, which could explain the disparate plateau (Huenke and Smith, 1976).

The youngest age reported from the vertical vein (13.22 ± 0.06 Ma, 1248-243C) is 0.2 m.y. older than the oldest age from the horizontal vein (13.02 ± 0.03 Ma, 1248-244B), confirming the field relationship of the horizontal vein crosscutting the vertical. Spatial analysis of the pattern of dates shows veins growing inwardly from both sides. Growth rates of the vein are calculated from the horizontal vein (~70–100 mm/m.y.) and the vertical vein (~25 mm/m.y.).

This variation in alunite growth rate is possibly due to a function of pressure on vein aperture. Recent work in the field of crystal growth shows that growth rate is increased under higher pressures as the fluid reaches an apparent supersaturation (Hong, 1997). The faster growth in the horizontal vein is presumably due to higher pressures resulting from lithostatic loading on the aperture. The vertical vein was under hydrostatic pressure and was likely to be open at the surface. Evidence of acidic fluids escaping the subsurface and cementing gravels, forming ferricretes and jarosite cemented gravels (jarocretes), are found in this area and imply an open system (Mote et al., 2001).

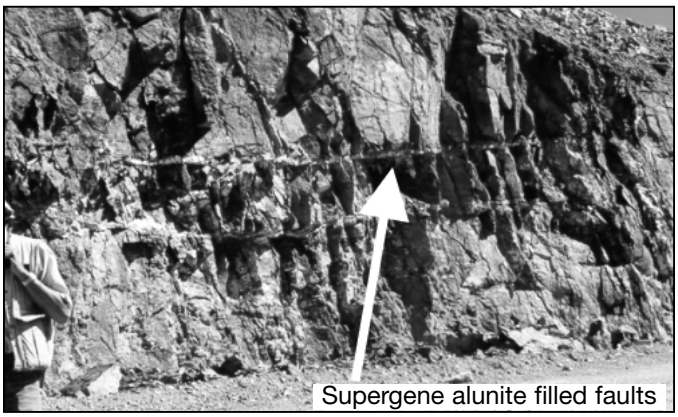

FIG. 6. Photograph of the paleospring feeder system, exposed by a roadcut, in the headwaters of Quebrada Riolita, viewing northeast toward Indio Muerto. Subhorizontal faults are filled with 10-cm supergene alunite veins.

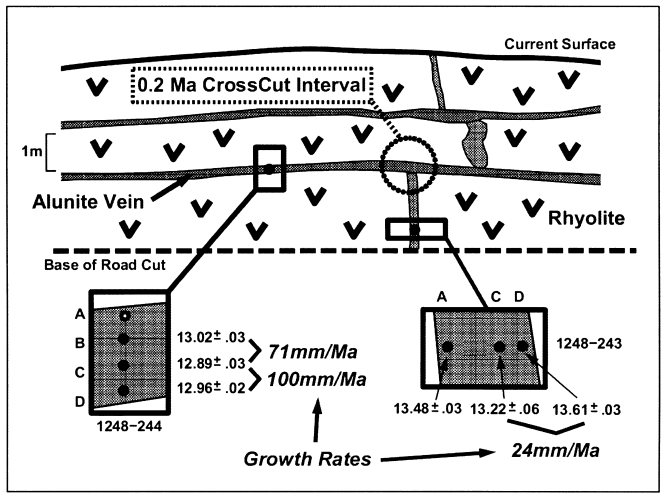

FIG. 7. Schematic diagram of the paleospring fault system (Fig. 6), showing the distribution of microsamples dated. Circled intersection illustrates a vertical vein cut by a horizontal vein with a 0.2 Ma difference in supergene alunite age. Individual growth rates for horizontal and vertical veins are shown.

Discussion

Feasibility of dating copper wad

Proper sample collection and separation of copper wad from the host material can produce ample samples for $^{40}Ar/^{39}Ar$ laser step-heating analysis. Characterization of copper wad shows that it is commonly in the cryptomelane and birnessite phases and generally contains over 1 wt percent K. Optical microscopy shows growth banding in samples, which are thought to represent individual mineralization events. The bands are commonly too narrow to microsample and, therefore, reported dates are an average of multiple growth generations. Scanning electron microscopy is necessary to not only characterize material being dated but to also identify for contaminants phases. Copper wad collected from open-space filling in bed rock is more likely to be contaminant free.

The cryptomelane (hollandite) structure has been shown to be argon retentive by other workers on many continents and in many different types of deposits (Vasconcelos et al., 1992, 1994; Lippolt and Hautmann, 1995; Dammer et al., 1996). Therefore, where the copper wad consists of cryptomelane, it may be readily dated to yield the age of formation of exotic copper deposits.

Although cryptomelane is found to be a component of copper wad mineralogy, birnessite is the more economic component of copper wad as it contains up to 20 wt percent copper in its layered structure and is the most abundant manganese oxyhydrate at El Salvador. The layered phyllomanganate structure of birnessite is not ideal for $^{40}Ar/^{39}Ar$ dating, because Ar retentivity is questionable, as noted by Vasconcelos et al. (1994). The hyperaridity of the Atacama presumably enhanced the retention of Ar, because limited fluid was available for cation exchange within the structure. Thus, birnessite appears to be feasible for $^{40}Ar/^{39}Ar$ dating under particular circumstances, which include limited postcrystallization ground-water interaction.

Although the majority of the age spectra presented for cryptomelane and birnessite show some minor discordance, plateau criteria are met for most of the samples. We conclude that discordance in the age spectra is due to postcrystallization argon loss and/or recoil effects. Argon loss is suggested by the ramping pattern of the low-temperature initial steps seen in many spectra of birnessite-rich copper wad. The Mn oxyhydrates have up to 7 stoichiometric molecules of H_2O which when heated volatize causing argon loss. Volatilization of H_2O may be due to high bake-out temperatures (8 h at 200°C) or irradiation temperatures (200°C). Argon loss from birnessite may be due to the open phyllomanganate structure, which is more susceptible to argon loss than the cryptomelane in the hollandite structure. Many of the age spectra show a humped pattern indicative of Ar recoil effects (Huneke and Smith, 1976). Recoil loss and redistribution of ^{39}Ar can be attributed to variations in density of individual growth bands, resulting from differences in composition, along with the small grain size of the copper wad minerals. Vasconcelos et al. (1994) have shown that recoil effects are negligible in cryptomelane. The high-temperature Ar release steps perhaps reflect degassing of more crystalline birnessite, which are apparently more Ar retentive.

Samples 1248-317-A (22.9 ± 0.3 Ma) and 1248-317-B (21.35 ± 0.15 Ma), adjacent pieces of a single birnessite vein, are similar but did not yield a reproducible plateau age within 1σ analytical error. Since the age spectra report an average of multiple mineralization events, due to the inability to separate individual growth bands, the results are interpreted as representing the same period of mineralization in the early Miocene and relevant in the context of this study.

Regardless of Ar loss or recoil effects, the majority of the samples do reach the plateau criteria of three continuous steps of over 50 percent of the gas within a 95 percent confidence (Fleck et al., 1977). We, therefore, conclude that $^{40}Ar/^{39}Ar$ dating is applicable to copper wad composed of the cryptomelane and K-rich birnessite phases and propose the addition of copper-bearing K birnessite to the list of minerals datable by $^{40}Ar/^{39}Ar$ laser step heating, but we acknowledge that further characterization of its behavior is necessary. At El Salvador, our data suggest that the apparent ages are a combination of multiple growth veins and may be a signal of the last fluid to move through the system as the hyperaridity of the Atacama preserved the mineral until today. In the context of exotic ore formation dating, it is the movement of this copper-bearing fluid with which we are concerned and, therefore, these dates are relevant to our interpretation.

Exotic mineralization at El Salvador

The exotic mineralization process at El Salvador began within 6 m.y. of the last hypogene mineralization event constrained to be approximately 41 Ma (Cornejo et al., 1997; Gustafson et al., 2001). The oldest date on copper wad at 35.35 ± 0.8 Ma (1248-448) implies that supergene enrichment processes were active at this time. This is consistent with the K-Ar dates on supergene alunite of 36.1 ± 0.6 and 36.0 ± 2.5 Ma by Gustafson and Hunt (1975). Our effort to apply the potentially more analytically accurate $^{40}Ar/^{39}Ar$ method to ascertain the inception age of supergene enrichment at El Salvador, by dating supergene alunite from the surface of the leached capping, proved inconclusive as the age spectrum in sample 1248-343 (Fig. 2) shown in Figure 4C is a climbing staircase best interpreted as a physical mixing of younger and older phases.

During the Oligocene and Miocene the timing of exotic Cu oxide mineralization was found beginning from about 25 Ma in the upper Oligocene until the youngest mineralization at about 11 Ma in the middle Miocene. In two cases, dates are correlative between the paleospring feeder from supergene alunite and exotic mineralization ages from copper wad, producing an independent check on these events. The mineralization at approximately 14 Ma in the middle Miocene is interpreted to be the main exotic mineralization event, as these processes can be correlated in multiple directions by five different sample locations (Fig. 5). Mineralization ceased at about 11 Ma and is preserved due to the aridification of the Atacama in the middle Miocene (Alpers and Brimhall, 1988).

As the precipitation of exotic ore minerals is mainly driven by an increase in pH (Munchmeyer, 1996), one may imagine a simple model of a reaction front altering the fresh rock and precipitating exotic minerals moving away from the source with time. The existence of four different ages (35.35 ± 0.80 (1248-448), 25.28 ± 0.4 (1248-449), 13.90 ± 0.20 (1248-9), and 11.05 ± 0.12 Ma (1248-232)) within an exploration shaft from Damiana and the two distinct ages (21.54 ± 0.17 (1248-450) and 14.40 ± 0.50 Ma (1248-451)) from parallel veins within 0.5 m of each other from a trench in Quebrada Turquesa, imply that exotic fluids of different ages follow similar recurrent paths.

Regional exotic copper genesis

Figure 8 shows an age probability diagram, using the method of Deino and Potts (1992), for all of the reported supergene ages at El Salvador (Gustafson and Hunt, 1975;

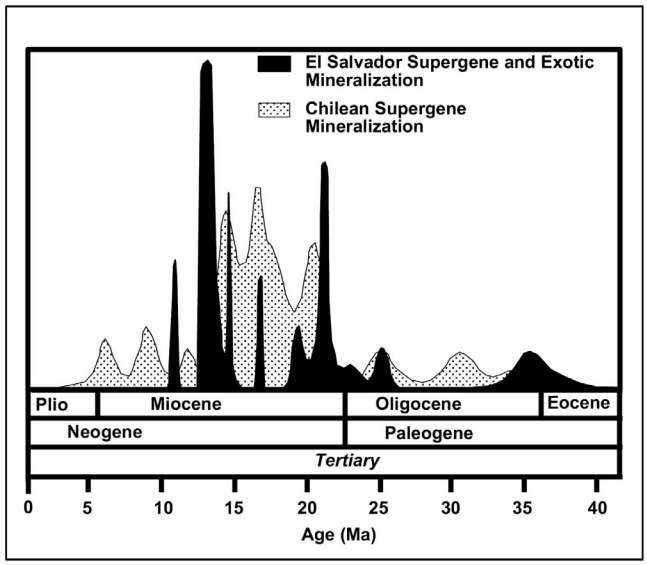

FIG. 8. Dating probability diagram, using the method of Deino and Potts (1992), of the El Salvador exotic and supergene enrichment (dark) and supergene mineralization throughout northern Chile (light). Notice the small peak at the Eocene-Oligocene boundary and the broad peak of mineralization beginning at the Oligocene-Miocene boundary continuing until the middle Miocene.

Sillitoe and McKee, 1996; this study) and all of the exotic and supergene mineralization ages in the Atacama desert of Chile excluding El Salvador (light; Alpers and Brimhall, 1988; Sillitoe and Mckee, 1996; Marsh et al., 1997). Both K-Ar and $^{40}Ar/^{39}Ar$ dates are presented. One should be aware that $^{40}Ar/^{39}Ar$ dates produce higher probability peaks as their analytical precision is greater than conventional K-Ar methods.

The overall pattern of supergene enrichment throughout northern Chile is similar to the local pattern of supergene and exotic mineralization seen at El Salvador. This supports the idea that supergene enrichment is driven by regional to global controls (Alpers and Brimhall, 1988; Vasconcelos et al., 1994; Brimhall and Mote, 1997).

The oldest supergene mineralization was enhanced by a global climate change near the Eocene-Oligocene boundary (Brimhall and Mote, 1997). Evidence of this older mineralization event may not be preserved as well as the younger events, because there are fewer source deposits of Eocene age, and this older mineralization presumably occurs at the top of the enrichment system, which is susceptible to erosion or further reworking.

The majority of supergene and exotic mineralization began near the Oligocene-Miocene boundary, correlated with an abrupt climate transition at this boundary (Zachos et al., 1994), and continued until the middle Miocene when enrichment stopped and was preserved due to the lack of infiltration meteoric water caused by desiccation of the Atacama (Alpers and Brimhall, 1988). The youngest evidence of supergene enrichment in northern Chile comes from Potrerillos where Marsh et al. (1997) dated supergene alunite at 9.10 ± 0.5 Ma and jarosite at 6.34 ± 0.5 Ma. This event is interpreted to represent the last mineralization at this latitude before desiccation preserved the supergene system as a geochemical fossil.

Acknowledgments

This study has been supported by a research grant to the University of California at Berkeley from CODELCO Chile to G. Brimhall.

At El Salvador thanks goes to Osman Olivares, Alicia Lehman, and Carlos Kreft who were particularly helpful in collecting the samples. We also acknowledge Marcelo Gomez for field support at the Exotica deposit. Special thanks go to John Dilles for providing the samples from the El Abra and Chuquicamata districts.

REFERENCES

Alpers, C.N., and Brimhall G.H, 1988, Middle Miocene climatic change in the Atacama desert, northern Chile: Evidence from supergene mineralization at La Escondida: Geological Society of America Bulletin, v. 100, p. 1640–1656.

Anderson, J.A., 1982, Characteristics of leached capping and techniques of appraisal, *in* Title, S.R., ed., Advances in the geology of porphyry copper deposits, southwestern North America: Tuscon, Arizona, University of Arizona Press, p. 275–295.

Brimhall, G.H, and Mote T.I., 1997, Optimal secondary mineralization in the Andes: Vadose response to global Cenozoic cooling events, glaciation, eustacy and desiccation [abs.]: Geological Society of America Abstracts with Programs, v. 29, no. 6, p. 17.

Carrasco, P., and Rojas, R., 1993, Geologia y evaluacion de recursos del yacimiento Damiana: Santiago, Chile, CODELCO, Unpublished company report.

Cornejo, P., Tosdal, R.M., Mpodozis, C., Tomlinson, A., Rivera, O., and Fanning, M.C., 1997, El Salvador, Chile, porphyry copper deposit revisited: Geologic and geochronologic framework: International Geology Review, v. 39, p 22–54.

Dammer D., Chivas, A.R., and McDougall, I., 1996, Isotopic dating of supergene manganese oxides from the Groote Eylandt deposit, Northern Territory, Australia: Economic Geology, v. 91, p. 386–401.

Deino, A.L., and Potts, R., 1992, Age-probability spectra for examination of single-crystal $^{40}Ar/^{39}Ar$ dating results: Examples from Olorgesailie, southern Kenya rift: Quaternary International, v. 13/14, p. 47–53.

Fam, R., 1979, Mineralization de cobre del tipo "exotico" en el norte de Chile: Chilean Geologic Congress, 2nd, Arica, Actas, v. 2, p. 235–263.

Fam, R.R., Kreft, C., Segovia, R., Rojas, O.O., Silva, W., Lehmann A., and Nur, P.J., 1997, Revaluacion Geologica-Proyecto Damiana: Santiago, Chile, CODELCO, Unpublished company report.

Fleck, R.J., Sutter, J.F., and Elliot, D.H., 1977, Interpretation of discordant $^{40}Ar/^{39}Ar$ age spectra of Mesozoic tholeiites from Antarctica: Geochimica et Cosmochimica Acta, v. 41, p. 15–32.

Gustafson, L.B., and Hunt, J.P., 1975, The porphyry copper deposit at El Salvador Chile: Economic Geology, v. 70, p. 857–912.

Gustafson, L.B., and Quiroga, G.J., 1995, Patterns of mineralization and alteration below the porphyry copper orebody at El Salvador, Chile: Economic Geology, v. 90, p. 2–16.

Gustafson, L.B., Orquera, W., McWilliams, M., Castro, M., Olivares, O., Rojas, G., Maluenda, J., and Mendez, M., 2001, Multiple centers of mineralization in the Indio Muerto district, El Salvador, Chile: Economic Geology, v. 96, p. 325–350.

Holland, K.L., and Walker, J.R., 1996, Crystal structural modeling of a highly disordered potassium birnessite: Clays and Clay Minerals, v. 44, p. 744–748.

Hong, J., 1997, Crystal growth in gravity: Journal of Crystal Growth, v. 181, p. 459–460.

Huneke, J.C., and Smith, S.P., 1976, The realities of recoil: ^{39}Ar out of small grains and anomalous patterns in $^{40}Ar/^{39}Ar$ dating: Geochimica et Cosmochimica Acta, v. 7, p. 1987–2008.

Itaya, T., Arribas, A., Jr., and Okada, T., 1996, Argon release systematics of hypogene and supergene alunite based on progressive heating experiments from 100 to 1000° C: Geochimica et Cosmochimica Acta, v. 60, p. 4525–4535.

Lippolt, H.J., and Hautmann, S., 1995, $^{40}Ar/^{39}Ar$ ages of Precambrian manganese ore minerals from Sweden, India and Morocco: Mineralium Deposita, v. 30, p. 246–256.

Marsh, T.M., Einaudi, M.T., and McWilliams, M., 1997, $^{40}Ar/^{39}Ar$ geochronolgy of Cu-Au and Au-Ag mineralization in the Potrerillos district, Chile: Economic Geology, v. 92, p. 784–806.

Mortimer, C., 1973, The Cenozoic history of the southern Atacama desert, Chile: Geological Society of London Journal, v. 129, p. 505–526.

Mortimer, C., Münchmeyer, F.C., and Urqueta, D.I., 1977, Emplacement of the Exotica orebody, Chile: Institution of Mining Metallurgy Transasctions, v. 86, sec. B, p. B121–B127.

Mote, T.I., 1999, Mass balance analysis and geochronology of exotic ore forming processes at the El Salvador porphyry copper deposit, Chile: Unpublished Ph.D. dissertation, Berkeley, CA, University of California, 169 p.

Mote, T.I., and Brimhall, G.H, 1997, Linking secondary mineralization at El Salvador, Chile to middle Miocene climate transitions by geochronolgy and mass balance [abs.]: Geological Society of America Abstracts with Programs, v. 29, no. 6, p. 17.

Mote, T.I., Brimhall, G.H, Tidy, F., E. Müller, G.H., and Carrasco, P., 2001, Application of Mass-Balance Modeling of Sources, Pathways, and Sinks of Supergene Enrichment to Exploration and Discovery of the Quebrada Turquesa Exotic Copper Orebody, El Salvador District, Chile: Economic Geology, v. 96, p. 367–386.

Münchmeyer, C., 1996, Exotic deposits—products of lateral migration of supergene solutions from porphyry copper deposits: Society of Economic Geologists Special Publication 5, p. 43–58.

Pino, J.H., 1997, Seguimiento del blanco Exotico Alicia proyecto de exploracion complejo domos S.E. Indio Muerto informe de avance 2 A.P.I. 961704: Santiago, Chile, CODELCO, Unpublished company report.

Post, J.E., and Veblen, D.R., 1990, Crystal structure determinations of synthetic sodium, Mg and K birnessite using TEM and the Rietveld method: American Mineralogist, v. 75, p. 477–489.

Renne, P.R., Swisher, C.C., Deino, A.L., Karner, D.B., Owens, T., and DePaolo, D.J., 1998, Intercalibration of standards, absolute ages and uncertainties in $^{40}Ar/^{39}Ar$ dating: Chemical Geology, v. 145, p. 117–152.

Reynolds, P., 1998, High-precision $^{40}Ar/^{39}Ar$ dating of two consecutive hydrothermal events in the Chuquicamata porphyry copper system, Chile: Chemical Geology, v. 148, p. 45–60.

Rojas, R., and Müller, G., 1994, "Damiana": Uno de los yacimientos tipo "Exoticos" de El Salvador: Congresso Geologico Chileno, 7th, Conception, 1994, Actas, v. 2, p. 892–896.
Sillitoe, R.H., and McKee, E.H., 1996, Age of supergene oxidation and enrichment in the Chilean porphyry copper deposit province: Economic Geology, v. 91, p. 164–179.
Sillitoe, R.H., Mortimer, C., and Clark, A.H., 1968, A chronology of landform evolution and supergene mineral alteration, southern Atacama desert, Chile: Institution of Minining and Metallurgy Transactions, v. 77, sec. B, p. B166–B169.
Smith, P.A. 1941, Minerals of the Butte district, Montana: Rocks and Minerals, v. 16, no. 7, p. 241–247.
Vasconcelos, P.M., Becker, T.A., Renne, P.R., and Brimhall, G.H, 1992, Age and duration of weathering by K-Ar and $^{40}Ar/^{39}Ar$ of potassium-manganese oxides: Science, v. 258, p. 451–454.
Vasconcelos, P.M., Renne, P.R., Brimhall, G.H, and Becker, T.A., 1994, Direct dating of weathering phenomena by $^{40}Ar/^{39}Ar$ and K-Ar analysis of supergene K-Mn oxides: Geochimica, v. 58, p. 1635–1665.
Zachos, J.C., Stott, L.D., and Lohmann, K.C., 1994, Evolution of the early Cenozoic marine temperatures: Paleoceanography, v. 9, p. 353–387.

APPENDIX I

$^{40}Ar/^{39}Ar$ Analysis of Copper Wad and Supergene Alunite from El Salvador, Chuquicamata and El Abra

Lab no.	Laser power (W)	$^{40}Ar/^{39}Ar$	$\%^{40}Ar^*$	Age (Ma)	$\pm 1\sigma$ (Ma)	^{40}Ar (moles)	$^{40}Ar^*/^{39}Ar$	$^{38}Ar/^{39}Ar$	$^{37}Ar/^{39}Ar$	$^{36}Ar/^{39}Ar$
1248-9 Birnessite					J = 0.0017722 ± 0.0000084					
10237-01A	0.02	115.298	–1.6	–5.846	3.856	3.70E-14	–1.826	0.0857	0.1381	0.3964
10237-01B	0.04	49.044	1.8	2.824	2.218	1.59E-14	0.884	0.0443	0.1487	0.163
10237-01C	0.08	19.493	4.8	2.997	1.078	5.94E-15	0.938	0.0246	0.1286	0.0628
10237-01D	0.12	10.257	26.5	8.683	0.955	2.53E-15	2.722	0.0183	0.1025	0.0255
10237-01E	0.16	8.277	41.8	11.018	0.628	2.98E-15	3.457	0.0171	0.1007	0.0163
10237-01F	0.22	7.202	61.4	14.088	0.411	3.96E-15	4.423	0.0141	0.0975	0.0094
10237-01G	0.28	6.405	70	14.28	0.426	3.18E-15	4.484	0.0126	0.0877	0.0065
10237-01H	0.34	5.979	70.5	13.424	0.594	1.87E-15	4.214	0.0117	0.078	0.006
10237-01I	0.42	5.776	68.3	12.565	0.743	1.33E-15	3.943	0.0121	0.0887	0.0062
10237-01J	0.5	5.757	52.6	9.661	1.052	6.06E-16	3.03	0.0101	0.1099	0.0093
10237-01K	0.6	5.035	62.1	9.964	1.945	4.39E-16	3.125	0.0149	0.125	0.0065
10237-01L	0.7	4.185	102.1	13.605	3.155	1.83E-16	4.271	0.0058	0.1112	–0.0003
10237-01M	0.8	4.62	–140.5	–20.869	5.282	1.25E-16	–6.49	0.0315	0.1962	0.0376
10237-01N	0.95	5.696	–134.8	–24.727	9.9	8.46E-17	–7.681	0.0437	0.4063	0.0454
10237-01O	1.1	3.093	–759	–76.636	24.339	2.00E-17	–23.471	0.0128	0.2761	0.089
10237-01P	1.3	2.255	–395.1	–28.707	36.605	9.57E-18	–8.908	0.052	0.2068	0.0378
10237-01Q	1.6	–0.32	–4075.2	41.327	38.133	-1.22E-18	13.074	0.1239	0	0
10237-01R	2	8.041	–426.8	–113.188	67.662	2.15E-17	–34.321	0.0551	0.1157	0.1434
10237-01S	2.6	5.181	560.9	90.616	21.009	3.79E-17	29.06	–0.0212	0.1899	–0.0808
10237-01T	3.5	16.959	646.6	320.619	133.1	2.22E-17	109.673	0.0273	0.2358	–0.3
1248-232	~90% Birnessite, 10% Cryptomelane				J = 0.0009252 ± 0.0000062					
10287-01A	0.25	103.274	–1.1	–1.842	2.118	3.53E-14	–1.103	0.0757	0	0.3532
10287-01B	0.05	1057.372	2.9	49.825	124.377	5.31E-14	30.263	0.6562	0.0897	3.475
10287-01C	0.1	224.685	3.5	13.022	4.425	1.34E-13	7.829	0.1548	0.0563	0.7339
10287-01D	0.2	89.472	4.8	7.182	1.406	1.02E-13	4.311	0.0692	0.0487	0.2882
10287-01E	0.275	36.671	8.3	5.103	1.013	2.31E-14	3.061	0.0345	0.0493	0.1137
10287-01F	0.375	23.469	13.5	5.275	0.739	1.81E-14	3.165	0.0245	0.0539	0.0687
10287-01G	0.5	10.839	59.8	10.792	0.255	1.68E-14	6.485	0.015	0.0452	0.0147
10287-01H	0.75	9.519	71.2	11.283	0.168	3.29E-14	6.78	0.0138	0.0379	0.0093
10287-01I	1	13.386	47	10.479	0.305	1.80E-14	6.296	0.0162	0.0597	0.024
10287-01J	1.25	14.883	30	7.434	0.878	6.30E-15	4.463	0.0197	0.1739	0.0353
10287-01K	1.5	14.005	41.2	9.612	3.186	1.59E-15	5.774	0.0144	0.219	0.0279
10287-01L	1.75	15.017	28.9	7.228	8.034	7.72E-16	4.339	0.0225	0.2099	0.0362
10287-01M	2	76.126	9.4	11.927	16.859	2.36E-15	7.169	0.0661	0.1502	0.2334
1248-448	Birnessite >> Cryptomelane				J = 0.0009099 ± 0.0000053					
10305-01A	0.035	–638.9818	82.8	–1186.746	8075.672	1.71E-16	–529.7474	0.3788956	2.331107	–0.3719331
10305-01B	0.1	811.2424	2.3	30.79334	25.36931	2.06E-13	18.91988	0.5295505	0.2817548	2.681381
10305-01C	0.2	222.9663	5.6	20.33698	6.21902	4.58E-14	12.4592	0.1492188	0.2460088	0.7124461
10305-01D	0.4	63.14746	31.3	32.15228	1.424526	1.92E-14	19.76238	4.21E-02	0.1930335	0.146877
10305-01E	0.55	37.48518	60.5	36.84552	1.024831	1.05E-14	22.67659	2.19E-02	0.1659437	5.02E-02
10305-01F	0.75	33.73722	67.1	36.80949	0.9669074	1.01E-14	22.65424	1.90E-02	0.1608412	3.76E-02
10305-01G	1	35.81306	56.3	32.82651	1.989076	4.97E-15	20.18052	2.42E-02	0.1778279	5.30E-02
10305-01H	1.5	42.29594	30.1	20.77371	1.826617	7.98E-15	12.72825	2.99E-02	0.2800031	0.1001396
10305-01I	2	67.52256	27.5	30.22494	5.204804	4.70E-15	18.56782	0.0391591	2.241272	0.1663552
10305-01J	2.5	338.7408	6.9	38.14874	111.3189	4.12E-15	23.48717	0.2142237	0.431613	1.066984
10305-01K	3	231.1616	–0.5	–2.048452	136.8469	1.66E-15	–1.247192	7.86E-02	0.7916576	0.786687
10305-01L	4	34.57796	7.1	33.39492	248.5985	1.29E-15	20.53331	0.1301242	1.112111	0.9148466

APPENDIX I *(Cont.)*

Lab no.	Laser power (W)	$^{40}Ar/^{39}Ar$	$\%^{40}Ar^*$	Age (Ma)	±1σ (Ma)	^{40}Ar (moles)	$^{40}Ar^*/^{39}Ar$	$^{38}Ar/^{39}Ar$	$^{37}Ar/^{39}Ar$	$^{36}Ar/^{39}Ar$
1248-449	Birnessite >>Cryptomelane				J = 0.0009163 ± 0.0000053					
10305-02A	0.025	681.759	11.4	123.615	445.634	1.51E-15	77.384	0.5447	0	2
10305-02B	0.05	1842.818	0	–0.752	250.118	3.14E-14	–0.455	1.176	0.0308	6.237
10305-02C	0.1	2247.555	0.5	18.847	81.827	2.19E-13	11.461	1.4173	0.3607	7.5673
10305-02D	0.2	2127.259	0.9	31.837	58.692	5.92E-13	19.43	1.3493	0.3307	7.1332
10305-02E	0.275	1503.46	0.5	11.831	33.788	4.67E-13	7.181	0.9601	0.3385	5.0636
10305-02F	0.375	315.805	1.7	8.705	5.91	1.27E-13	5.279	0.2085	0.2676	1.0509
10305-02G	0.5	132.326	10.1	21.955	1.989	7.02E-14	13.363	0.0886	0.2433	0.4027
10305-02H	0.75	48.718	30.8	24.637	0.655	4.05E-14	15.006	0.0336	0.1918	0.1141
10305-02I	1	46.692	33.3	25.534	0.719	2.86E-14	15.556	0.0322	0.3027	0.1055
10305-02J	1.25	73.599	23.8	28.776	1.578	1.76E-14	17.547	0.0497	2.4304	0.1904
10305-02K	1.5	147.352	12.6	30.623	4.946	1.15E-14	18.683	0.0958	3.9111	0.4366
10305-02L	1.75	191.577	12.9	40.658	9.581	8.46E-15	24.874	0.1199	5.0997	0.5658
10305-02M	2	277.703	8.6	39.005	21.312	7.50E-15	23.851	0.1775	4.6642	0.8606
1248-244A	Supergene alunite				J = 0.0009097 ± 0.0000054					
10310-02A	1	644.893	2.4	25.326	31.978	2.79E-13	15.539	0.4173	0.0176	2.1298
10310-02B	2	74.614	13.2	16.112	0.974	7.94E-13	9.861	0.0539	0	0.2191
10310-02C	2.4	21.801	38.8	13.824	0.237	4.47E-13	8.455	0.0204	0	0.0452
10310-02D	2.8	15.359	53.4	13.402	0.163	4.39E-13	8.196	0.0168	0.0005	0.0242
10310-02E	3.2	12.67	63.9	13.23	0.137	3.92E-13	8.091	0.0151	0.0002	0.0155
10310-02F	3.6	11.417	71.6	13.37	0.124	3.74E-13	8.177	0.0141	0.0004	0.011
10310-02G	4	10.412	79.6	13.557	0.113	3.30E-13	8.291	0.0133	0	0.0072
10310-02H	4.8	10.307	83.2	14.013	0.114	3.15E-13	8.571	0.0134	0	0.0059
10310-02I	5.6	10.998	84	15.099	0.119	3.80E-13	9.239	0.0134	0	0.006
10310-02J	6.4	14.263	74.2	17.295	0.675	3.24E-14	10.588	0.0141	0	0.0124
1248-244B	Supergene alunite				J = 0.0009097 ± 0.0000054					
10311-01A	1	123.204	4.1	8.359	2.916	8.48E-14	5.105	0.0906	0	0.3997
10311-01B	2	12.6	63.7	13.119	0.12	2.84E-13	8.022	0.0154	0.0024	0.0155
10311-01C	2.4	8.999	88.5	13.022	0.088	5.72E-13	7.963	0.013	0.0022	0.0035
10311-01D	2.8	8.703	91.4	13.01	0.087	5.71E-13	7.956	0.0126	0.0015	0.0025
10311-01E	3.2	9.09	89.4	13.291	0.092	3.57E-13	8.128	0.0128	0.001	0.0033
10311-01F	3.6	9.961	80.4	13.09	0.149	1.26E-13	8.004	0.0136	0.0001	0.0066
10311-01G	4	11.563	70.5	13.321	0.506	3.35E-14	8.147	0.015	0	0.0116
10311-01H	4.8	14.454	61.1	14.426	1.604	1.23E-14	8.825	0.0145	0	0.019
10311-01I	6	18.103	41.7	12.355	2.424	1.05E-14	7.554	0.0232	0	0.0357
10311-01J	6	18.789	42	12.912	2.104	1.24E-14	7.896	0.0155	0	0.0369
1248-244C	Supergene alunite				J = 0.0009097 ± 0.0000054					
10312-01A	1	88.153	160.4	218.373	65.88	8.44E-16	141.383	0.0696	0	–0.1801
10312-01B	2	14.057	34.1	7.844	0.881	9.83E-15	4.79	0.0182	0.0133	0.0314
10312-01C	2.4	8.751	79.5	11.38	0.226	2.43E-14	6.956	0.0132	0.0117	0.0061
10312-01D	2.8	8.552	91.5	12.803	0.116	5.79E-14	7.829	0.0126	0.0046	0.0024
10312-01E	3.2	8.392	94.6	12.98	0.106	7.65E-14	7.937	0.0122	0.0039	0.0015
10312-01F	3.6	8.322	95.4	12.987	0.098	1.06E-13	7.942	0.0124	0.0039	0.0013
10312-01G	4	8.223	97.2	13.065	0.089	2.40E-13	7.989	0.0122	0.0042	0.0008
10312-01H	4.8	8.151	96.7	12.888	0.086	3.96E-13	7.881	0.0123	0.0044	0.0009
10312-01I	6	8.156	96.7	12.891	0.085	5.72E-13	7.882	0.0121	0.0044	0.0009
10312-01J	6	7.938	94.3	12.244	0.136	9.87E-14	7.485	0.0121	0.0034	0.0015
1248-244D	Supergene alunite				J = 0.0009097 ± 0.0000054					
10313-01A	1	39.326	–2.6	–1.68	2.688	1.06E-14	–1.023	0.0313	0.0019	0.1365
10313-01B	2	10.767	65.7	11.57	0.15	6.88E-14	7.072	0.0145	0.0008	0.0125
10313-01C	2.4	8.688	93	13.21	0.097	1.30E-13	8.078	0.0124	0.002	0.0021
10313-01D	2.8	8.418	94.5	13.009	0.09	2.00E-13	7.955	0.0122	0.0014	0.0016
10313-01E	3.2	8.353	95.2	12.998	0.088	2.69E-13	7.948	0.0125	0.0019	0.0014
10313-01F	3.6	8.254	96.3	12.992	0.086	3.58E-13	7.945	0.0124	0.0017	0.001
10313-01G	4	8.244	95.9	12.931	0.086	3.54E-13	7.907	0.0121	0.0015	0.0011
10313-01H	4.8	8.161	97	12.94	0.086	3.99E-13	7.912	0.0122	0.0012	0.0008
10313-01I	6	8.139	97.1	12.923	0.088	3.85E-13	7.902	0.0122	0.0012	0.0008
10313-01J	6	8.413	92.9	12.778	0.139	1.08E-13	7.813	0.0123	0.0004	0.002
1248-243C	Supergene alunite				J = 0.0009097 ± 0.0000054					
10315-01A	1	309.64	2.7	13.801	51.786	3.10E-14	8.441	0.1988	0	1.0193
10315-01B	2	98.774	5.1	8.286	1.651	3.49E-13	5.06	0.0709	0	0.3171
10315-01C	2.4	26.297	31.2	13.424	0.365	2.41E-13	8.209	0.024	0	0.0612
10315-01D	2.8	15.81	50.7	13.103	0.191	2.57E-13	8.013	0.0172	0.0003	0.0264

APPENDIX I *(Cont.)*

Lab no.	Laser power (W)	$^{40}Ar/^{39}Ar$	$\%^{40}Ar^*$	Age (Ma)	±1σ (Ma)	^{40}Ar (moles)	$^{40}Ar^*/^{39}Ar$	$^{38}Ar/^{39}Ar$	$^{37}Ar/^{39}Ar$	$^{36}Ar/^{39}Ar$
10315-01E	3.2	13.255	61.1	13.248	0.155	3.00E-13	8.101	0.0147	0.0005	0.0174
10315-01F	3.6	12.803	63.2	13.232	0.138	3.62E-13	8.092	0.0154	0.0006	0.0159
10315-01G	4	14.059	57.8	13.288	0.151	4.18E-13	8.126	0.0163	0.0005	0.0201
10315-01H	4.8	17.696	46.2	13.357	0.19	5.15E-13	8.169	0.0184	0.0007	0.0322
10315-01I	6	19.881	38.6	12.566	0.294	1.81E-13	7.683	0.0196	0	0.0413
10315-01J	6	21.614	39.2	13.857	0.231	6.54E-13	8.475	0.02	0.0005	0.0445
1248-243A	Supergene alunite					J = 0.0009097 ± 0.0000054				
10316-01A	1	62.986	3.1	3.229	4.675	1.65E-14	1.969	0.045	0	0.2065
10316-01B	2	13.744	49.5	11.125	0.219	4.49E-14	6.799	0.0167	0	0.0235
10316-01C	2.4	10	78.6	12.857	0.131	5.81E-14	7.862	0.0134	0	0.0072
10316-01D	2.8	8.964	92	13.486	0.1	1.07E-13	8.248	0.0126	0	0.0024
10316-01E	3.2	8.685	94	13.346	0.095	1.30E-13	8.162	0.0124	0.0002	0.0018
10316-01F	3.6	8.568	95.3	13.345	0.092	1.60E-13	8.161	0.0123	0.0003	0.0014
10316-01G	4	8.534	96.3	13.441	0.09	2.07E-13	8.22	0.0122	0.0003	0.0011
10316-01H	6	8.595	96.2	13.519	0.089	5.29E-13	8.268	0.0125	0.0006	0.0011
10316-01I	6	30.294	32.1	15.891	4.232	1.04E-14	9.725	0.0295	0	0.0696
1248-243D	Supergene alunite					J = 0.0009097 ± 0.0000054				
10317-01A	0.5	55.08	–7.8	–7.067	57.63	1.10E-15	–4.298	0.0803	0.0463	0.201
10317-01B	1	43.693	7.6	5.426	2.287	1.84E-14	3.311	0.0376	0.0019	0.1367
10317-01C	1.5	14.044	37.3	8.58	0.306	3.00E-14	5.241	0.0179	0.0004	0.0298
10317-01D	2	9.347	79.4	12.138	0.119	6.54E-14	7.42	0.0134	0.0002	0.0065
10317-01E	2.5	8.775	93.3	13.389	0.097	1.22E-13	8.188	0.0127	0.0008	0.002
10317-01F	3	8.644	96.5	13.632	0.091	2.34E-13	8.337	0.0123	0.0007	0.001
10317-01G	3.5	8.55	97.3	13.604	0.09	2.80E-13	8.32	0.0123	0.0005	0.0008
10317-01H	4	9.118	90.9	13.547	0.107	9.12E-14	8.285	0.0128	0.0004	0.0028
10317-01I	4.5	10.855	79.8	14.153	0.374	1.54E-14	8.657	0.0139	0	0.0074
10317-01J	5	26.463	40.6	17.554	3.217	5.07E-15	10.748	0.0251	0.0046	0.0532
1248-450	Birnessite					J = 0.0025256 ± 0.0000094				
11021-02A	0.25	103.416	1.6	7.488	3.408	1.07E-13	1.647	0.0784	0.1354	0.3444
11021-02B	0.375	34.109	5.4	8.422	1.119	4.56E-14	1.853	0.0352	0.1504	0.1092
11021-02C	0.5	15.122	21.2	14.558	0.513	3.79E-14	3.208	0.0213	0.1558	0.0404
11021-02D	0.675	10.045	47.9	21.814	0.262	4.31E-14	4.817	0.0166	0.142	0.0177
11021-02E	0.85	9.076	51.7	21.269	0.256	3.45E-14	4.696	0.0158	0.1351	0.0149
11021-02F	1.05	9.031	45.9	18.795	0.409	1.51E-14	4.146	0.0154	0.1462	0.0166
11021-02G	1.25	9.452	37.3	15.999	1.486	2.62E-15	3.527	0.0168	0.1078	0.0201
11021-02H	1.5	14.519	19.3	12.734	12.904	4.19E-16	2.805	0.0172	4.0408	0.0407
11021-02I	1.75	17.993	52.4	43.411	81.601	8.09E-17	9.642	0.0034	30.7028	0.0371
11021-02J	2.5	19.582	52.4	46.231	26.447	2.52E-16	10.277	0.0289	2.5088	0.0322
1248-317-B	Birnessite					J = 0.0025256 ± 0.0000094				
11023-01A	0.03	354.194	2.9	46.101	654.253	4.568E-15	10.246	0.2190	0.2188	1.1640
11023-01B	0.05	313.298	1.4	19.244	41.644	6.165E-14	4.245	0.2192	0.2114	1.0459
11023-01C	0.1	513.730	0.3	6.462	32.869	2.841E-13	1.421	0.3419	0.1574	1.7337
11023-01D	0.2	314.204	1.3	19.003	13.926	3.216E-13	4.192	0.2190	0.1398	1.0491
11023-01E	0.28	99.232	5.2	23.546	4.455	9.531E-14	5.200	0.0760	0.1582	0.3183
11023-01F	0.38	37.729	11.4	19.522	1.222	7.101E-14	4.307	0.0361	0.1618	0.1131
11023-01G	0.5	18.602	26.5	22.336	0.595	6.033E-14	4.932	0.0220	0.1371	0.0463
11023-01H	0.75	12.475	41.3	23.353	0.388	4.697E-14	5.158	0.0173	0.1374	0.0248
11023-01I	1	9.148	38.5	15.983	1.077	6.795E-15	3.523	0.0162	0.1644	0.0191
11023-01J	1.25	6.992	53.0	16.818	2.064	2.590E-15	3.708	0.0147	0.1265	0.0111
11023-01K	1.5	7.029	72.2	22.992	9.795	5.969E-16	5.077	0.0092	0.1528	0.0066
11023-01L	1.75	6.909	62.8	19.669	14.965	3.016E-16	4.340	0.0145	0.1619	0.0087
11023-01M	2.25	8.032	66.5	24.196	14.817	3.476E-16	5.345	0.0127	0.0722	0.0091
1248-317-B	Birnessite					J = 0.0025256 ± 0.0000094				
11023-02A	0.125	619.131	–0.1	–3.381	72.109	2.35E-13	–0.741	0.4083	0.1319	2.097
11023-02B	0.25	454.766	–1.1	–22.742	24.408	6.65E-13	–4.96	0.307	0.1511	1.555
11023-02C	0.375	187.65	0	–0.384	6.686	6.60E-13	–0.084	0.1377	0.1435	0.6353
11023-02D	0.5	142.383	1.3	8.495	4.886	5.07E-13	1.869	0.1067	0.1462	0.4756
11023-02E	0.75	84.206	3.3	12.718	2.605	5.40E-13	2.801	0.0674	0.1505	0.2755
11023-02F	1	34.511	11.6	18.112	1.011	3.71E-13	3.995	0.0337	0.1531	0.1033
11023-02G	1.25	20.354	22.2	20.476	0.509	3.30E-13	4.519	0.0237	0.1429	0.0536
11023-02H	1.5	17.469	26.8	21.217	0.429	2.63E-13	4.684	0.0216	0.1425	0.0433
11023-02I	1.75	17.011	27.8	21.419	0.467	1.25E-13	4.729	0.0215	0.1467	0.0416
11023-02J	2.25	11.055	42	21.046	0.275	1.06E-13	4.646	0.0173	0.135	0.0217

APPENDIX I *(Cont.)*

Lab no.	Laser power (W)	$^{40}Ar/^{39}Ar$	$\%^{40}Ar^*$	Age (Ma)	±1σ (Ma)	^{40}Ar (moles)	$^{40}Ar^*/^{39}Ar$	$^{38}Ar/^{39}Ar$	$^{37}Ar/^{39}Ar$	$^{36}Ar/^{39}Ar$
11023-02K	3	9.042	53.3	21.831	0.259	6.33E-14	4.82	0.0155	0.1531	0.0143
1248-QD168B	Hydrothermal sericite					J = 0.0025256±0.0000094				
11025-03A	0.25	377.886	0.6	10.528	21.151	1.23E-13	2.317	0.2559	0	1.271
11025-03B	0.375	258.277	4.1	47.515	11.674	1.19E-13	10.566	0.2056	0.134	0.8383
11025-03C	1	23.235	28.7	30.179	0.496	1.55E-13	6.679	0.0242	0.1403	0.0561
11025-03D	0.675	14.698	59.8	39.581	1.375	5.66E-15	8.782	0.0166	0.0773	0.02
11025-03E	0.85	9.893	80.3	35.848	0.422	1.12E-14	7.946	0.0144	0.1302	0.0066
11025-03F	1.05	9.298	83.9	35.183	0.291	2.18E-14	7.797	0.013	0.0599	0.0051
11025-03G	1.25	9.057	84.8	34.659	0.255	2.28E-14	7.68	0.0136	0.0414	0.0047
11025-03H	1.5	9.685	81.5	35.614	0.229	3.14E-14	7.894	0.0141	0.0683	0.0061
11025-03I	1.75	10.929	71.5	35.24	0.26	5.02E-14	7.81	0.0144	0.0529	0.0106
11025-03J	2.5	11.259	69.6	35.361	0.223	7.08E-14	7.837	0.0147	0.0476	0.0116
1248-QD168A	Hydrothermal sericite					J = 0.0025256 ± 0.0000094				
11025-04A	0.25	125.681	5.3	30.165	3.463	1.66E-13	6.676	0.0966	0.1712	0.4028
11025-04B	0.375	23.368	22	23.289	0.819	3.50E-14	5.144	0.0249	0.1028	0.0617
11025-04C	0.5	12.587	58	32.968	0.617	1.29E-14	7.302	0.017	0.1279	0.0179
11025-04D	0.675	9.909	79.9	35.72	0.486	9.57E-15	7.917	0.0141	0.2187	0.0068
11025-04E	0.85	9.265	83.7	34.977	0.494	1.02E-14	7.751	0.0135	0.1342	0.0052
11025-04F	1.05	9.847	79.7	35.427	0.603	7.90E-15	7.852	0.0141	0.1491	0.0068
11025-04G	1.25	10.711	77.1	37.234	0.701	8.22E-15	8.256	0.0149	0.1334	0.008
11025-04H	1.5	11.028	72.1	35.867	0.508	1.23E-14	7.95	0.0148	0	0.0104
11025-04I	1.75	10.712	73	35.272	0.452	1.29E-14	7.817	0.0147	0	0.0098
11025-04J	2.5	10.485	75.7	35.791	0.482	1.06E-14	7.933	0.0144	0.0076	0.0086
1248-QD89	Cryptomelane					J = 0.0025256 ± 0.0000094				
11026-02A	0.25	294.886	–0.6	–8.569	36.933	2.69E-14	–1.876	0.2085	0	1.0043
11026-02B	0.375	210.993	0.4	3.837	8.588	1.56E-13	0.843	0.147	0	0.7112
11026-02C	1	64.666	3.2	9.436	1.397	8.09E-13	2.076	0.0526	0.0159	0.2118
11026-02D	0.675	33.108	9.1	13.628	1.045	5.64E-14	3.002	0.0315	0.0439	0.1019
11026-02E	0.85	22.068	18.5	18.511	0.567	8.41E-14	4.083	0.0239	0.0102	0.0609
11026-02F	1.05	12.81	40.3	23.364	0.253	1.08E-13	5.161	0.0173	0.0036	0.0259
11026-02G	1.25	8.24	65.1	24.274	0.142	1.79E-13	5.363	0.0139	0.0117	0.0097
11026-02H	1.5	5.94	77	20.712	0.099	2.89E-13	4.572	0.013	0.0055	0.0046
11026-02I	1.75	4.623	81.4	17.065	0.075	4.36E-13	3.763	0.0128	0.0063	0.0029
11026-02J	2.5	4.248	88.3	17.01	0.071	7.50E-13	3.751	0.0124	0.0067	0.0017
1248-451	Birnessite					J = 0.0025256 ± 0.0000094				
11029-02A	0.125	350.032	0.9	14.324	64.474	5.50E-14	3.156	0.2388	0.082	1.1739
11029-02B	0.25	218.943	0	–0.16	15.107	1.00E-13	–0.035	0.1559	0.0938	0.7411
11029-02C	0.375	150.144	0.8	5.506	10.946	9.32E-14	1.21	0.1107	0.0987	0.504
11029-02D	0.5	88.823	1.7	6.675	4.812	8.06E-14	1.468	0.0719	0.1106	0.2956
11029-02E	0.75	52.8	5	11.953	2.045	1.30E-13	2.632	0.0454	0.1079	0.1698
11029-02F	1	36.538	8.2	13.637	1.167	1.44E-13	3.004	0.0339	0.1007	0.1135
11029-02G	1.25	30.984	10.2	14.356	1.038	1.11E-13	3.163	0.0314	0.0998	0.0942
11029-02H	1.5	26.615	13	15.749	1.014	7.49E-14	3.472	0.0275	0.0954	0.0783
11029-02I	1.75	22.848	14.2	14.693	1.461	2.45E-14	3.238	0.025	0.0957	0.0664
11029-02J	2.25	22.36	15.4	15.671	3.129	9.68E-15	3.454	0.0231	0.0963	0.064
11029-02K	3	19.054	10.2	8.814	7.817	3.03E-15	1.939	0.0231	0.103	0.0579
1248-336	K-Silicate					J = 0.0025256 ± 0.0000094				
11036-04A	0.25	97.044	12.3	53.642	8.69	1.30E-14	11.949	0.0757	0.1237	0.288
11036-04B	0.375	21.494	39.7	38.491	1.511	9.56E-15	8.538	0.0258	0.1041	0.0439
11036-04C	0.5	9.777	85.6	37.745	0.499	8.95E-15	8.371	0.0137	0	0.0048
11036-04D	0.675	8.46	96.2	36.721	0.389	9.64E-15	8.141	0.0122	0	0.0011
11036-04E	0.85	8.176	96.7	35.65	0.258	1.53E-14	7.902	0.0116	0	0.0009
11036-04F	1.05	8.125	97	35.565	0.247	1.77E-14	7.883	0.0123	0	0.0008
11036-04G	1.25	8.279	95.6	35.691	0.265	1.52E-14	7.911	0.0125	0	0.0012
11036-04H	1.5	8.413	92.4	35.079	0.201	2.80E-14	7.774	0.0123	0	0.0022
11036-04I	1.75	8.412	93	35.284	0.185	4.44E-14	7.82	0.0125	0	0.002
11036-04J	2.5	8.392	93.5	35.402	0.157	1.23E-13	7.846	0.0126	0	0.0018
1248-343	Supergene/Hypogene Alunite					J = 0.0025256 ± 0.0000094				
11037-01A	1.6	109.124	0.6	3.17	4.224	3.39E-13	0.696	0.0825	0.047	0.3669
11037-01B	2.4	24.691	22.3	24.864	0.615	3.17E-13	5.495	0.0245	0.0211	0.065
11037-01C	2.8	14.619	49.6	32.722	0.328	1.28E-13	7.247	0.0171	0.0154	0.025
11037-01D	3.2	13.153	59.7	35.405	0.266	1.66E-13	7.847	0.0157	0.014	0.018

APPENDIX I *(Cont.)*

Lab no.	Laser power (W)	$^{40}Ar/^{39}Ar$	$\%^{40}Ar^*$	Age (Ma)	$\pm 1\sigma$ (Ma)	^{40}Ar (moles)	$^{40}Ar^*/^{39}Ar$	$^{38}Ar/^{39}Ar$	$^{37}Ar/^{39}Ar$	$^{36}Ar/^{39}Ar$
11037-01E	3.6	12.417	65.6	36.757	0.254	1.44E-13	8.149	0.0151	0.0132	0.0144
11037-01F	4	11.912	70.7	37.955	0.243	1.31E-13	8.418	0.0144	0.012	0.0118
11037-01G	4.8	11.869	71.9	38.49	0.235	1.35E-13	8.538	0.0144	0.0116	0.0113
11037-01H	5.6	12.057	70.8	38.49	0.237	1.36E-13	8.538	0.0145	0.0118	0.0119
11037-01I	6.4	11.839	73	38.943	0.242	1.21E-13	8.639	0.0144	0.0117	0.0108
11037-01J	6.4	11.822	73.6	39.225	0.225	1.72E-13	8.703	0.0143	0.0115	0.0106
1248-318	Supergene Alunite					J = 0.0025090 ± 0.0000089				
11044-01A	1.6	23.349	6.4	6.734	7.593	2.72E-15	1.491	0.0243	0	0.074
11044-01B	2.4	8.628	35.1	13.654	0.404	1.93E-14	3.028	0.0159	0.0186	0.019
11044-01C	2.8	7.663	39.7	13.724	0.313	2.57E-14	3.043	0.0152	0.0203	0.0156
11044-01D	3.2	7.626	39.6	13.623	0.279	2.94E-14	3.021	0.0153	0.0202	0.0156
11044-01E	3.6	7.575	40.5	13.817	0.258	3.51E-14	3.064	0.0151	0.0205	0.0153
11044-01F	4	7.67	39.8	13.747	0.251	3.83E-14	3.049	0.0151	0.0211	0.0156
11044-01G	4.8	7.262	43.1	14.1	0.214	4.84E-14	3.127	0.0144	0.0213	0.014
11044-01H	5.6	7.295	44	14.46	0.203	5.54E-14	3.207	0.0151	0.0227	0.0138
11044-01I	6.4	7.313	43.8	14.435	0.186	6.66E-14	3.202	0.015	0.0225	0.0139
11044-01J	7	7.469	41.6	13.992	0.185	8.22E-14	3.103	0.0149	0.0223	0.0148
1248-327	Supergene Alunite					J = 0.0025090 ± 0.0000089				
11053-01A	1	56.09	2.8	7.082	5.65	2.67E-14	1.568	0.0581	0.0715	0.1845
11053-01B	1.5	11.686	34.1	17.958	0.6	2.30E-14	3.987	0.0171	0.0334	0.0261
11053-01C	2	7.338	57.1	18.853	0.375	1.98E-14	4.187	0.0132	0.0306	0.0107
11053-01D	2.5	6.69	56.3	16.963	0.38	1.80E-14	3.765	0.0135	0.0375	0.0099
11053-01E	3.25	8.671	35	13.666	0.575	1.58E-14	3.031	0.0178	0.0586	0.0191
11053-01F	4.5	40.358	4	7.292	4.683	1.79E-14	1.614	0.0481	0.184	0.1312
11053-01G	5.5	10224.71	–4	0	143547900	2.01E-15	–407.634	7.5103	0	3
11053-01H	7	–3192.431	–3.1	401.281	36689	9.55E-15	99.205	–1.9901	2.4851	–11.13
1248-433	Cryptomelane					J = 0.0018005 ± 0.0000093				
11121-02A	0.25	213.762	2.2	15.3	18.62	1.69E-14	4.73	0.1445	0.3802	0.7075
11121-02B	0.375	261.62	1.1	8.921	7.693	1.72E-13	2.753	0.1805	0.3782	0.8761
11121-02C	0.5	224.871	1.9	13.976	4.496	3.72E-13	4.319	0.1552	0.332	0.7465
11121-02D	0.675	165.242	1.9	10.094	3.628	3.11E-13	3.116	0.1177	0.2981	0.5487
11121-02E	0.85	115.285	2.7	10.043	2.283	2.46E-13	3.1	0.0873	0.2831	0.3797
11121-02F	1.05	71.235	4.9	11.258	1.301	2.17E-13	3.477	0.0588	0.2661	0.2294
11121-02G	1.25	35.12	9.4	10.743	0.678	1.61E-13	3.317	0.0336	0.2528	0.1077
11121-02H	1.5	15.077	27.2	13.253	0.215	2.43E-13	4.095	0.0199	0.231	0.0372
11121-02I	1.75	9.794	49.4	15.65	0.138	1.73E-13	4.839	0.0153	0.209	0.0168
11121-02J	2.5	8.007	64.3	16.651	0.108	3.10E-13	5.15	0.0137	0.1789	0.0097